Intelligent Signal Processing Routine for Instantaneous Heart Rate Detection using a Six-Port Microwave Interferometer

Christoph Will, Kilin Shi, Fabian Lurz, Robert Weigel, and Alexander Koelpin
Institute for Electronics Engineering, University of Erlangen-Nuremberg
Cauerstr. 9, 91058 Erlangen, Germany
Email: christoph.will@fau.de

***Abstract*—Instantaneous heart rate detection is one of the key parameters in medical vital parameter monitoring. In medical centers e.g., real time monitoring of the vital signs of a patient under surveillance is necessary. Nowadays, the dominant technologies are electrocardiogram (ECG) or ballistocardiogram (BCG), but the required direct contact to the person-under-surveillance is a common drawback of these sensors. In this paper, a Six-Port microwave interferometer is presented and used to detect the current heart rate of a person-under-test. An intelligent signal processing routing is proposed that avoids the fast Fourier transform (FFT) due to the implicated longsome observation window and operates directly in the time domain instead. A commercial ECG product is used to proof the reliability of the presented signal processing routine to establish Six-Port microwave interferometers for instantaneous heart rate detection.**

Keywords*—Six-Port, Interferometers, Biomedical signal processing, Heartbeat monitoring.

I. Introduction

In modern society real time monitoring of vital signs gets more and more important. Real time monitoring in this case means continuously detecting the present heartbeat and breath rates with minimal delay. The purpose is to immediately detect abnormalities, malfunction or even failure of heart and lung. A common example is a cardiac arrest in the hospital, whereby a doctor has to start reanimation as fast as possible. However, not only in medical centers vital sign monitoring is useful, but there exists a variety of application cases. Parents benefit from the surveillance of their babies since it facilitates an early detection of sleep apnea or the Sudden Infant Death Syndrome (SIDS) [1], which is still one of the major causes of infant death, especially in the first year of life [2]. Another application area is in automobiles where the health status of the driver can be monitored. As fully autonomous driving is not yet ready for the market, the next step to increase safety are driver health monitoring systems. Due to a heart attack or a hypoglycemic shock, the driver loses the control over the vehicle, which could lead to deathly accidents. The detection of these events can start an emergency routine to prevent such a scenario and stop the car safely.

Over the years, different methods for vital sign detection have been researched and developed. The most common and established method for heartbeat monitoring is the ECG due to its high accuracy and reliability. The drawback of this system is the necessity of at least two electrodes on the skin. More comfortable can be pulse oximetry based systems that monitor the oxygen saturation by measuring changes of light absorbance on the finger-tip by photodetectors [3]. Systems integrated in air mattresses do not have fixed contact with the patient and are even able to detect breathing. Two variants are the pneumatic method where the pressure on the mattress is measured [4] and a phonocardiogram [5]. Since the 1970s contact-free measurement has been enabled by continues wave (CW) radar systems, which exploited the Doppler shift [6] as the thorax is expanded by breathing as well as the vasodilative blood wave on upper skin layers. First approaches had a poor performance, but the technique improved over the years [7]. As simple CW radar systems can only measure relative distances, enhanced variations have been developed, like frequency modulated continues wave (FMCW) radars [8]. Whereas CW radar systems use one carrier frequency, respectively a frequency ramp, ultra wideband (UWB) systems send signal pulses with a bandwidth of several mega- to gigahertz. Six-Port microwave interferometers depict a CW radar sub-group with a very precise phase resolution. This technique is presented in detail in Sec. II.

Common radar sensors use the FFT to determine the major spectral components. In case of vital sign detection the heartbeat and breath rate are the desired output signals. However, harmonics of the breath signal can interfere with the heartbeat component or body movements can generate a disturbing peak in the spectrum. In consideration of real-time capability an inevitable observation window of 10 s...30 s for an appropriate frequency resolution depicts another drawback. For these reasons intelligent signal processing has to be applied to facilitate accurate heart rate estimation directly in the time domain. Autocorrelation-based methods have already been studied for a 2.4 GHz Doppler radar [9], in this paper an adjusted and improved approach is presented for a 24 GHz Six-Port interferometer. Vital sign detection in this frequency region by Six-Port sensors have already been published [10] as well as fast and simple algorithms in the time domain for automotive application cases [11]. Hereby, an intelligent signal routine is proposed to enhance the accuracy, robustness, and update rate of the system.

II. Measurement Principle

The Six-Port network was introduced for power measurement applications by Engen and Hoer in the 1970s [12]. Since then the technology has been enhanced more and more and

other application cases have emerged [13]. Nowadays it is known as a phase evaluating receiver setup for (sub-)millimeter frequencies. Two of the six ports are fed with input signals $\underline{P_1}$ and $\underline{P_2}$ that are superimposed by one Wilkinson power divider and three quadrature hybrid couplers. The complete passive structure delivers four output signals $\underline{P_3}$ to $\underline{P_6}$ with a static phase shift of $\pi/2$ amongst each other. A schematic of the Six-Port network is illustrated in Fig. 1.

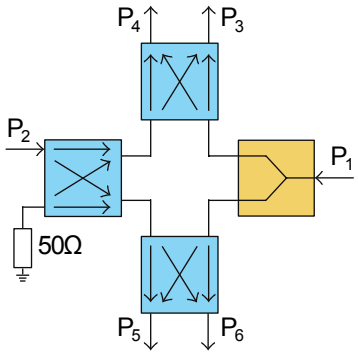

Fig. 1. Circuit schematic of the Six-Port network.

Within a Six-Port microwave interferometer one input signal of the network is the emitted signal, the other is the received signal reflected at the target. With f being the carrier frequency the two complex input signals $\underline{P_1}$ and $\underline{P_2}$ can be defined as:

$$\begin{aligned}\underline{P_1} &= A_1 \cdot e^{j(2\pi f t+\phi_1)} \\ &= A_1 \cdot [\cos(\omega t+\phi_1) + j\sin(\omega t+\phi_1)] \\ \underline{P_2} &= A_2 \cdot e^{j(2\pi f t+\phi_2)} \\ &= A_2 \cdot [\cos(\omega t+\phi_2) + j\sin(\omega t+\phi_2)]\end{aligned} \tag{1}$$

A_1 and A_2 represent the amplitudes, ω is radial frequency $2\pi f$, and ϕ_1 resp. ϕ_2 are the phase values. Considering the relative phase differences of 0, $\pi/2$, π and $3\pi 2$ at the output ports, the complex output signals $\underline{P_3}$ to $\underline{P_6}$ can be calculated as:

$$\begin{aligned}\underline{P_3} &= 0.5 \cdot (\underline{P_1} + j\underline{P_2}) \\ \underline{P_4} &= 0.5 \cdot (j\underline{P_1} + \underline{P_2}) \\ \underline{P_5} &= 0.5 \cdot (j\underline{P_1} + j\underline{P_2}) \\ \underline{P_6} &= 0.5 \cdot (\underline{P_1} - \underline{P_2})\end{aligned} \tag{2}$$

Power detectors connected to the output ports cause a direct conversion to the baseband resulting in the square of the absolute power values. The system presented in this paper uses Schottky diodes delivering the baseband voltages $\underline{B_3}$ to $\underline{B_6}$:

$$\begin{aligned}B_3 &= \left|\underline{P_3}\right|^2 = 0.25 \cdot \left|\underline{P_1} + j\underline{P_2}\right|^2 \\ B_4 &= \left|\underline{P_4}\right|^2 = 0.25 \cdot \left|j\underline{P_1} + \underline{P_2}\right|^2 \\ B_5 &= \left|\underline{P_5}\right|^2 = 0.25 \cdot \left|j\underline{P_1} + j\underline{P_2}\right|^2 \\ B_6 &= \left|\underline{P_6}\right|^2 = 0.25 \cdot \left|\underline{P_1} - \underline{P_2}\right|^2\end{aligned} \tag{3}$$

Since the relative phase shift between the four output signals are multiples of $\pi/2$, the baseband signals can be transformed into a complex representation $\underline{Z}$. Both, the in-phase and the quadrature component, can be split up in differential pairs with a relative phase shift of π in between:

$$\underline{Z} = I + jQ = (B_5 - B_6) + j(B_3 - B_4) \tag{4}$$

The relative phase shift $\Delta\sigma$ between the two input ports $\underline{P_1}$ and $\underline{P_2}$ is represented by the argument of the complex expression $\underline{Z}$:

$$\Delta\sigma = \phi_1 - \phi_2 = \arg\{\underline{Z}\} \tag{5}$$

Since the wavelength λ of the carrier frequency is known, the relative distance of the target can be calculated using $\Delta\sigma$:

$$\Delta x = \frac{\Delta\sigma}{2\pi} \cdot \frac{\lambda}{2} \tag{6}$$

This signal represents the raw distance data which has to be further processed to extract the heart rate.

III. Signal Processing Routine

In comparison to ECG signals the raw received signal of the Six-Port microwave interferometer has a very low signal-to-noise ratio (SNR) regarding heartbeat extraction. Hence, an intelligent signal processing is necessary for an accurate heart rate estimation, which likewise has to be very fast to approach real-time capability. The complete flow chart of the proposed signal processing routine is illustrated in Fig. 2.

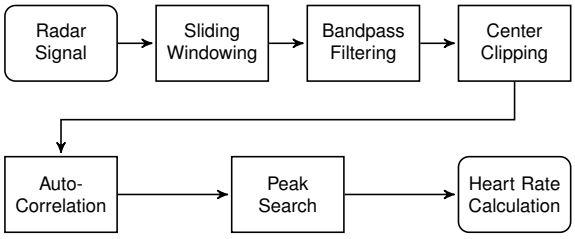

Fig. 2. Flow chart of the signal processing routine.

First of all, a sliding windowing is applied to the received signal since only the most recent part has to be examined. The length of the window and the update rate are parameters free to chose, depending on the result priorities as there is a trade-off between accuracy and actuality. A large window size implicates a higher accuracy, but also increases further signal processing delay. Additionally, as the heart rate may increase or decrease during the measurement the change is recognized with even more delay. In laboratory experiments best results have been achieved with a window length of only 6 s...8 s with an update every second.

The current cut-out (Fig. 3a) is bandpass filtered to suppress noise as well as the breath signal and letting pass the heartbeat signal (Fig. 3b). A fourth-order butterworth filter with 0.7 Hz as lower and 2.5 Hz as upper cut-out frequency has been chosen. Since a butterworth filter distorts the phase of the signal, what is unbearable for phase evaluation, the filter is passed a second time from the other direction, resulting in zero-phase filtering with no group delay.

The extracted heartbeat signal still has undesired peaks, which are removed by subsequent center clipping (Fig. 3c). In this stage, every value within a certain margin $k \cdot a_{max}$ around zero is set to zero:

$$\begin{aligned} c(n) &= 0 \qquad \forall\, |s(n)| \leq k \cdot a_{max} \\ &= s(n) \quad \forall\, |s(n)| > k \cdot a_{max} \end{aligned} \tag{7}$$

The values greater than the predefined margin are the only non-zero elements of the output signal $c(n)$. The margin consists of the maximal measured amplitude for a filtered heartbeat signal in the experimental phase (here: $a_{max} = 0.2$) and an additional threshold factor. The factor $k = 0.4$ has proven as suitable in practice and has also been used for the example illustrated in Fig. 3. Here, the effects of the first steps of the signal processing routine on the original signal are demonstrated.

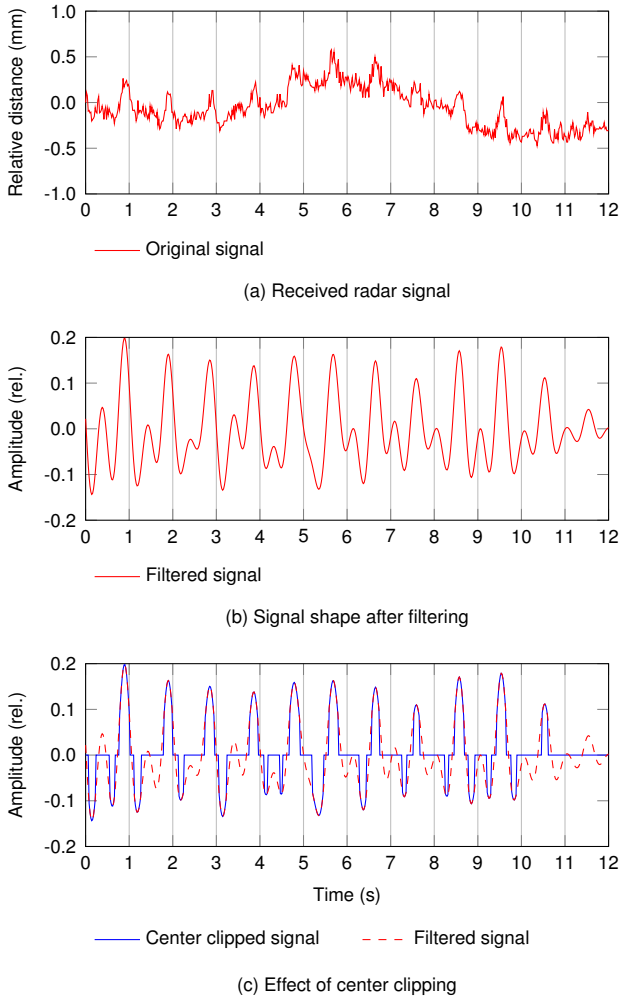

Fig. 3. Effects of the individual signal processing steps: signal shape of the raw distance data (a), after bandpass filtering (b) and after center clipping (c).

An important part of the signal processing routine is the autocorrelation of the center clipped signal in the following stage. The autocorrelation function (ACF) of a time discrete signal $x(\tau)$ in general is defined as:

$$\psi_{xx}(\tau) = \lim_{M \to \infty} \frac{1}{2M+1} \sum_{\nu=-M}^{M} x(\nu) \cdot x(\nu + \tau) \tag{8}$$

The autocorrelation is the cross-correlation of a signal with itself, which implicates an similarity analyses with itself. Thus, the ACF emphasizes the characteristics of a signal, like repeating patterns or periodic signals. During the autocorrelation process one of the overlaying signal copies is shifted in both directions above the other copy. As the ACF is a symmetric function, in the proposed routine the copy is shifted with the lag τ only in one direction. At $\tau = 0$ the ACF reaches its maximum, representing the point in time furthest in the past. The larger τ gets the more up-to-date the values become, however, the local maxima decreases for an increasing lag. In addition, new unwanted local maxima are generated, since the distance between the peaks of the center clipped signal varies due to the heart rate variability. Therefore, an advanced peak search algorithm is necessary.

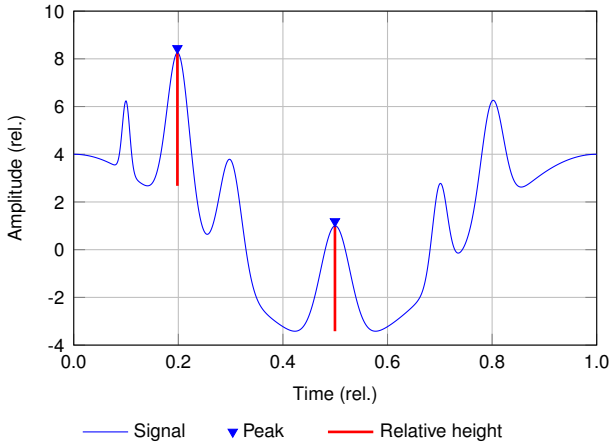

Fig. 4. Demonstration of the relative height used by peak search algorithm.

Due to the global maximum of the ACF at $\tau = 0$, the first peak is defined at this position. During peak search every local maximum, but also all local minima, are detected and recorded. For every maximum its *relative height* is calculated, which represents the height of the maximum in comparison to the greater neighbor minima on both sides. An exemplary visualization of the *relative height* is shown in Fig. 4. The detected maximum is only saved if its relative height is at least half as big as the previously detected maximum and additionally, if the lag difference to that maximum is greater or equal than 0.4 times the sampling rate F_s. The secondary condition avoids the wrong interpretation of sporadic noise peaks as heartbeats and is calculated out of the upper cut-off frequency of the bandpass filter (2.5 Hz). The autocorrelation of the center clipped signal of Fig. 3 together with the maxima identified by the proposed peak search algorithm is illustrated in Fig. 5.

In a final step the heart rate f_{HR} is calculated using the distances Δx between the detected peaks. Again, the user can decide on the number of peaks to take under consideration, weighing accuracy and actuality. With $\overline{\Delta x}$ being the mean of the considered peak distances, the current heart rate can be determined as:

$$f_{HR} = \frac{F_a}{\overline{\Delta x}} \tag{9}$$

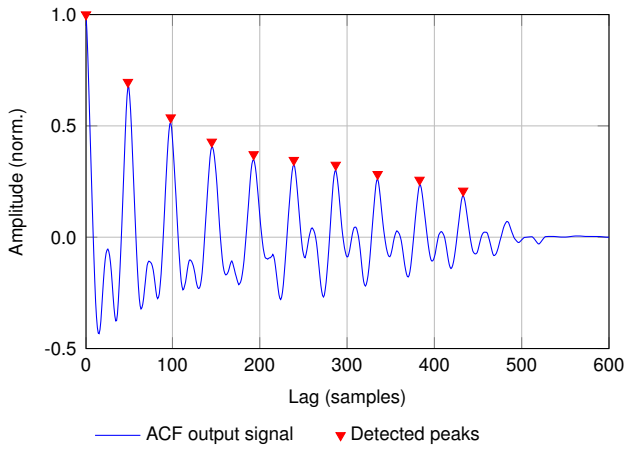

Fig. 5. Autocorrelation signal and the detected peaks.

IV. Experimental Setup and Measurement Results

The experimental setup to verify the functionality of the proposed signal processing routine is shown in Fig. 6. A compact Six-Port microwave interferometer [14] can be seen in the foreground of the photograph, focused on the person-under-test in front of the table. Inside the blue box the whole interferometer system is stashed, consisting of the high frequency front-end together with a 24 GHz reference source and a four-by-four patch antenna array, the Six-Port network, and the baseband circuitry. The integrated microcontroller samples the baseband voltages with a 12 bit analog-to-digital converter (ADC), calculates the relative distances and communicates via a serial connection. The signal processing routine to extract the heart rate is executed on a laptop which is connected to the Six-Port sensor by a USB-to-Serial adapter.

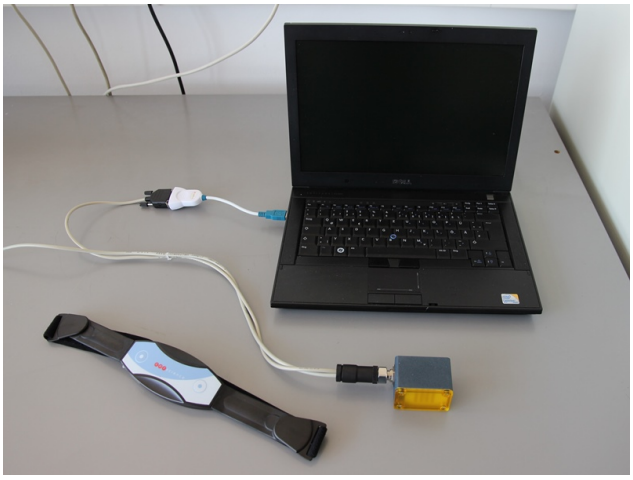

Fig. 6. Exemplary measurement system.

Next to the Six-Port sensor in Fig. 6 a common one-channel ECG chest belt is depicted. During the verification phase it was used for simultaneous measurements with the microwave interferometer. Due to the complete different signal shape resulting from the different physiological stimuli for ECG and distance monitoring, the ECG data was analyzed with another algorithm to determine the heart rate. A suitable signal processing routine for ECG signals is the well-known Pan-Tompkins-Algorithm [15]. It was developed in year 1985 by Jiapu Pan and Willis J. Tompkins to detect the significant QRS complex. A comparison of the determined heart rate (HR) in beats per minute (bpm) between both measurement systems is shown in Fig. 7. To emphasize the importance of intelligent signal processing routines, the result of the heart rate determination without center clipping is included, too. Only the five latest detected peaks were used for every heart rate calculation.

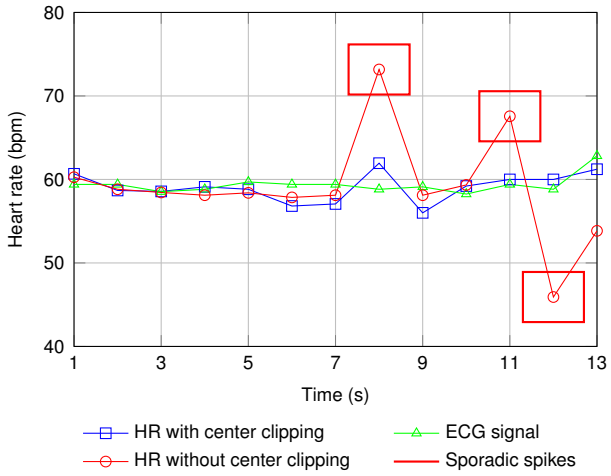

Fig. 7. Measurement results.

The heart rate comparison in Fig. 7 clearly demonstrates the improvement with the proposed routine. Without center clipping e.g., sporadic spikes exist, which appear especially when the SNR is low regarding the amplitude of the heartbeat signal. Hereby, simple autocorrelation would deliver a wrong periodicity, since parts of the noise signal preponderate and lead to higher peaks in the ACF. Applying the complete proposed signal processing routine delivers an appropriate heart rate accuracy in comparison to the commercial ECG product. The mean heart rate determined by the microwave interferometer is 59.5 bpm and thereby only 0.3 bpm higher than the mean heart rate detected by the ECG measurement (59.2 bpm). This confirms the functionality of the proposed routine together with the Six-Port microwave interferometer.

V. Conclusion

Nowadays, a fast and accurate measurement of the human heartbeat is required for a lot of application cases, e.g., in medical centers for patient monitoring or in automobiles as driver monitoring systems. Since comfort and mobility became important factors in modern society, contact-free measurement systems got favored in recent years. In this paper, a 24 GHz microwave interferometer based on the Six-Port network was presented to be used for instantaneous heart rate detection. An intelligent signal processing routine was proposed to provide significant accuracy and reliability, but also to achieve real-time capability. In several sub-steps the noisy received signal is extensively processed by excerpting the heartbeat signal, exploiting characteristic features and intelligently detecting

heartbeat peaks to determine the current heart rate. The reliability of the proposed signal processing routine was proven by comparison to a reference setup based on a commercial ECG product. Additionally, the enhancement by center clipping, regarding the resulting heart rate determination, was shown as an example for the importance of the single sub-steps. The experimental measurements confirm the suitability of the proposed signal processing routine for instantaneous heart rate detection using a Six-Port microwave interferometer.

REFERENCES

[1] P. Peirano, B. Signh, J. Lacombe, H. Cherrier, and N. Monod, "Cardiorespiratory patterns during sleep and wakefulness in infants who subsequently died of sids," in *Engineering in Medicine and Biology Society, 1988. Proceedings of the Annual International Conference of the IEEE*, Nov 1988, pp. 1930–1931 vol.4.

[2] C. E. Hunt and F. R. Hauck, "Sudden infant death syndrome," *Canadian Medical Association Journal*, vol. 174, no. 13, pp. 1861–1869, 2006.

[3] B.-H. Yang and S. Rhee, "Development of the ring sensor for healthcare automation," *Robotics and Autonomous Systems*, vol. 30, no. 3, pp. 273–281, 2000.

[4] K. Watanabe, T. Watanabe, H. Watanabe, H. Ando, T. Ishikawa, and K. Kobayashi, "Noninvasive measurement of heartbeat, respiration, snoring and body movements of a subject in bed via a pneumatic method," *Biomedical Engineering, IEEE Transactions on*, vol. 52, no. 12, pp. 2100–2107, Dec 2005.

[5] D. Balasubramaniam and D. Nedumaran, "Design and development of digital signal processor based phonocardiogram system," in *Signal Acquisition and Processing, 2010. ICSAP '10. International Conference on*, Feb 2010, pp. 366–370.

[6] J. C. Lin, "Microwave sensing of physiological movement and volume change: A review," *Bioelectromagnetics*, vol. 13, no. 6, pp. 557–565, 1992.

[7] O. Boric-Lubecke, V. Lubecke, B.-K. Park, W. Massagram, and B. Jokanovic, "Heartbeat interval extraction using doppler radar for health monitoring," in *Telecommunication in Modern Satellite, Cable, and Broadcasting Services, 2009. TELSIKS '09. 9th International Conference on*, Oct 2009, pp. 139–142.

[8] L. Anitori, A. de Jong, and F. Nennie, "Fmcw radar for life-sign detection," in *Radar Conference, 2009 IEEE*, May 2009, pp. 1–6.

[9] B. Lohman, O. Boric-Lubecke, V. Lubecke, P. Ong, and M. Sondhi, "A digital signal processor for doppler radar sensing of vital signs," in *Engineering in Medicine and Biology Society, 2001. Proceedings of the 23rd Annual International Conference of the IEEE*, vol. 4, 2001, pp. 3359–3362 vol.4.

[10] G. Vinci, S. Lindner, F. Barbon, S. Mann, M. Hofmann, A. Duda, R. Weigel, and A. Koelpin, "Six-port radar sensor for remote respiration rate and heartbeat vital-sign monitoring," *Microwave Theory and Techniques, IEEE Transactions on*, vol. 61, no. 5, pp. 2093–2100, May 2013.

[11] G. Vinci, T. Lenhard, C. Will, and A. Koelpin, "Microwave interferometer radar-based vital sign detection for driver monitoring syst," in *Microwaves for Intelligent Mobility (ICMIM), 2015 IEEE MTT-S International Conference on*, April 2015, pp. 1–4.

[12] G. F. Engen and C. A. Hoer, "Application of an arbitrary 6-port junction to power-measurement problems," *Instrumentation and Measurement, IEEE Transactions on*, vol. 21, no. 4, pp. 470–474, Nov 1972.

[13] S. Tatu and K. Wu, "Six-port technology and applications," in *Telecommunication in Modern Satellite, Cable and Broadcasting Services (TELSIKS), 2013 11th International Conference on*, vol. 01, Oct 2013, pp. 239–248.

[14] S. Linz, G. Vinci, S. Mann, S. Lindner, F. Barbon, R. Weigel, and A. Koelpin, "A compact, versatile six-port radar module for industrial and medical applications," *Journal of Electrical and Computer Engineering*, vol. 2013, p. 2, 2013.

[15] J. Pan and W. J. Tompkins, "A real-time qrs detection algorithm," *Biomedical Engineering, IEEE Transactions on*, vol. BME-32, no. 3, pp. 230–236, March 1985.